ELSEVIER

Journal of Photochemistry and Photobiology A: Chemistry 110 (1997) 1–10

Journal of PHOTOCHEMISTRY AND PHOTOBIOLOGY A: CHEMISTRY

Atmospheric fate of methyl vinyl ketone and methacrolein [1]

Tomasz Gierczak [a,b,2], James B. Burkholder [a,b], Ranajit K. Talukdar [a,b], A. Mellouki [a,b,3], S.B. Barone [a,b], A.R. Ravishankara [a,b,4]

[a] *NOAA, Aeronomy Laboratory, 325 Broadway, Boulder, CO 80303, USA*

[b] *The Cooperative Institute for Research in Environmental Sciences, University of Colorado, Boulder, CO 80309, USA*

Received 19 November 1996; revised 29 April 1997; accepted 12 May 1997

Abstract

The rate coefficients for the reaction of OH with methyl vinyl ketone (MVK, $CH_3C(O)CHCH_2$) and methacrolein (MACR, $CH_2C(CH_3)CHO$) between 232 and 378 K were measured using the pulsed laser photolysis–pulsed laser induced fluorescence (PP–PLIF) technique. The rate coefficient data can be expressed in the Arrhenius form as $k_1(OH + MVK) = (2.67 \pm 0.45) \times 10^{-12} \exp((452 \pm 130)/T)$ and $k_2(OH + MACR) = (7.73 \pm 0.65) \times 10^{-12} \exp((379 \pm 46)/T)$ cm^3 $molecule^{-1}$ s^{-1}, where the error limits are 2σ and include estimated systematic errors. The UV absorption cross-sections of MVK and MACR were measured over the wavelength range 250–395 nm using a diode array spectrometer. Absolute quantum yields for loss of MVK and MACR were measured at 308, 337, and 351 nm. The MACR quantum yield, Φ_{MACR}, was < 0.01. The MVK quantum yield was both pressure and wavelength dependent and is represented by the expression: $\Phi_0(\lambda,P) < \exp[-0.055(\lambda - 308)]/(5.5 + 9.2 \times 10^{-19}N)$ where λ is measured in nm and N is the number density in molecule cm^{-3}. Atmospheric loss rate calculations using these results show that the primary loss process for both MVK and MACR is the reaction with OH radicals throughout the troposphere. © 1997 Elsevier Science S.A.

Keywords: Methyl vinyl ketone; Methacrolein; OH rate coefficient; Absorption cross section; Quantum yield

1. Introduction

Isoprene ($CH_2CHC(CH_3)CH_2$) is the most abundant non-methane hydrocarbon (NMHC) emitted into the troposphere. The primary source of atmospheric isoprene is emission from trees. The atmospheric oxidation of isoprene, through its reactions with OH radicals, O_3, or NO_3, plays an important role in the production of ozone in both urban and rural areas [1,2]. The impact of isoprene emissions requires an understanding of the fate of not only isoprene but also its reaction products. Methyl vinyl ketone (MVK, $CH_3C(O)CHCH_2$) and methacrolein (MACR, $CH_2C(CH_3)CHO$) have been observed in both field and laboratory studies as major products in the oxidation of isoprene [3–5].

The oxidation of MVK and MACR through either reaction with OH or UV photolysis in the atmosphere leads to the formation of free radicals, PAN (peroxyacetyl nitrate), and ozone. There have been several studies of the OH reaction rate coefficients with MVK and MACR [6–9].

$$OH + CH_3C(O)CHCH_2\ (MVK) \rightarrow \text{products} \quad (1)$$

$$OH + CH_2C(CH_3)CHO\ (MACR) \rightarrow \text{products} \quad (2)$$

Cox et al. [8], Edney et al. [9], and Atkinson et al. [7] used relative rate techniques to study reactions (1) and (2) at room temperature. Kleindienst et al. [6] used a flash photolysis resonance fluorescence technique to study reactions (1) and (2) at 298, 350, and 424 K. The reported room temperature values for reaction (1) are in reasonable agreement, within 25%, and fall into the range $(1.5–2) \times 10^{-11}$ cm^3 $molecule^{-1}$ s^{-1}. The reported room temperature values for reaction (2) have about the same level of agreement with values in the range $(3–4) \times 10^{-11}$ cm^3 $molecule^{-1}$ s^{-1}. The limited amount of temperature dependent data restricts the accuracy of extrapolations to the lower temperatures found in the troposphere. Therefore, accurate measurements over a wider temperature range are desired.

The UV absorption spectra of MVK and MACR have been reported in several studies [10–12]. The agreement among these studies is reasonably good with both molecules having

[1] Some of the results described here were presented at an SPIE meeting in Berlin, Germany, 1992.

[2] Present address: Department of Chemistry, Warsaw University, ul. Zwirki i Wigury 101, 02-089 Warszawa, Poland.

[3] Present address: LCSR/CNRS, 45071 Orleans Cedex 02, France.

[4] Also affiliated with: Department of Chemistry and Biochemistry, University of Colorado, Boulder, CO 80309, USA.

PII S1010-6030(97)00159-7

relatively weak, $< 10^{-19}$ cm^2 molecule^{-1}, continuous bands centered near 330 nm. Although the absorption cross-sections are relatively small, the high solar flux in this wavelength range leads to a short atmospheric photolysis lifetime provided the photolysis quantum yield is unity. Raber and Moortgat [10] have recently measured the photolysis quantum yields for MVK and MACR to be significantly less than one. They report upper limits of 0.03 and 0.05 for the quantum yields for MACR and MVK, respectively. Even with these small quantum yields, photolysis would be a significant loss process in the atmosphere. Therefore, better absolute limits and the wavelength dependence of the quantum yields are required to critically evaluate this atmospheric loss process.

In this paper, we report the OH reaction rate coefficients with MVK and MACR as a function of temperature and the UV absorption cross sections and photolysis quantum yields of MVK and MACR. The improved accuracy of these measurements enables a more quantitative evaluation of the atmospheric loss processes of MVK and MACR.

2. Experimental section

The experimental apparatus and techniques used to study the OH kinetics and UV absorption spectra of MVK and MACR have been described in detail in previous publications [13,14]. Therefore, only a brief description is given below. The techniques used to study the photolysis quantum yields are given in detail in a separate section.

2.1. OH kinetic measurements

The rate coefficients for the reaction of OH with MVK and MACR, were measured over the temperature range 232–378 K using the technique of pulsed laser photolysis–pulsed laser induced fluorescence (PP–PLIF). The apparatus consists of a pyrex reactor (150 cm^3 internal volume), a pulsed laser for the OH source and a pulsed laser induced fluorescence detection method for OH.

The temperature of the reactor was regulated to 1 K by circulating a fluid from a thermostated bath through its jacket. The temperature of the gas stream flowing through the reactor was measured with a retractable thermocouple in the volume defined by the intersection of the photolysis and the probe laser beams. The temperature of the gases was the same as the temperature of the circulating fluid. The lower limit of the temperature range for kinetic measurements was determined by the vapor pressure of the OH precursor, H_2O_2.

OH radicals were produced by pulsed photolysis of H_2O_2 at either 248 nm (KrF laser) or 266 nm (fourth harmonic of Nd:YAG laser) where the OH quantum yield is two [15]. The initial OH concentration was varied during the measurements by a factor of 4 by changing the H_2O_2 concentration and/or the photolysis laser fluence (1.4–12.5 mJ cm^{-2} pulse^{-1}). The absorption cross-sections of MVK and MACR at 248 nm are $< 2.5 \times 10^{-21}$ cm^2 molecule^{-1} and at 266 nm are $< 5 \times 10^{-21}$ cm^2 molecule^{-1}. The ratio of $[H_2O_2]$ to [MVK] or [MACR] was typically between 0.1 and 1. The absorption cross-sections of H_2O_2 at 248 and 266 nm are 9×10^{-20} and 7×10^{-20} cm^2 molecule^{-1}, respectively [16]. Therefore, the radical concentrations generated from MVK or MACR photolysis were at least ten times smaller than that of OH, assuming a quantum yield for MVK and MACR photolysis of one (see discussion section). The kinetic results were independent of the photolysis wavelength used.

The OH signal was measured using pulsed laser induced fluorescence as a function of the time delay between the photolysis and probe laser pulses. The OH temporal profiles were measured under pseudo first order conditions, [MVK] or $[MACR] > 10^3[OH]_o$, such that:

$$[OH]_t/[OH]_o = \exp(-k't) \quad (3)$$

where $k' = k_1[\text{reactant}] + k_d$ and k_d is the first-order rate coefficient (s^{-1}) for the loss of OH in the absence of the reactant. The large [reactant]/[OH] ratios used also minimizes the effect of OH reaction with reaction products. Linear least-squares analysis of the ln[OH] versus t data were used to determine k'. The values of k_1 were obtained by the linear least-squares analysis of k' at various reactant concentrations.

The concentrations of MVK and MACR flowing through the reactor were measured via absorption at 213.86 nm (Zn lamp) in 25 cm long absorption cells located before and after the reactor. The concentrations measured before the reactor were found to be within 1–2% of those measured after the reactor at all temperatures.

The rate coefficients for the reactions of OH with MVK and MACR are relatively large, $> 10^{-11}$ cm^3 molecule^{-1} s^{-1}, so that OH reaction with minor impurities do not make a significant contribution to the measured values of k_1 and k_2. The largest impurity in the samples is hydroquinone which is used as a stabilizer. However, hydroquinone has a negligible vapor pressure and was separated from the samples by vacuum distillation.

2.2. UV absorption cross-section measurements

The collimated output of a 30W D_2 lamp was passed through a 25.3 cm long absorption cell and focused onto the entrance slit of a 0.25 m spectrometer with a 1024 element diode array detector. The wavelength of the spectrometer was calibrated using a Hg pen ray lamp. The estimated uncertainty in the wavelength was 0.2 nm. The resolution was ~0.5 nm. The cross-sections were measured over the range 190–420 nm. Measurements at wavelengths longer than 250 nm used a longpass cut-off filter mounted between the light source and absorption cell to eliminate photolysis of MVK and MACR in the absorption cell during the spectrum measurement. Without optical filtering, observable decreases in the MVK and MACR and the formation of other absorbing species were detected on the time scale of minutes. Measurements were made over the temperature range of 250–298 K.

Spectra were measured by summing 100 scans, each scan consisting of a 50 ms exposure of the diode array. The reference spectrum (I_0) was recorded with the absorption cell purged with He. The MVK or MACR sample was introduced into the cell and a second spectrum (I) was recorded. Absorption cross-sections were obtained via:

$$\sigma(\lambda) = -\ln[I(\lambda)/I_0(\lambda)]/LN \quad (4)$$

where $\sigma(\lambda)$ is the UV absorption cross-section (cm^2 molecule^{-1}) at wavelength λ, L is the pathlength in cm, and N is the number density of the absorber in molecule cm^{-3}.

Uncertainties in the measured optical pathlength, temperature, pressure, and absorbance contribute to the overall uncertainty in the measured absorption cross-sections. The pathlength, temperature, and pressure measurements each are uncertain by ~1%. The baseline fluctuations were <0.1%, as determined by measuring $I_0(\lambda)$ before filling and after pumping out the absorption cell. The precision of the measurements was ±2% RMS. We estimate the absolute uncertainty to be ±5% RMS (2σ) at the peak of the spectra increasing to 15% in the wings.

The absorption cross-sections of MVK and MACR were also measured to be $(6.6 \pm 0.35) \times 10^{-18}$ cm^2 molecule^{-1} and $(2.21 \pm 0.11) \times 10^{-17}$ cm^2 molecule^{-1}, respectively at the 213.86 nm Zn line. The quoted uncertainties are 2σ and include estimated systematic errors. The absorption cross-sections were measured using a Zn pen ray lamp, either a 100 or 2 cm long absorption cell, and a photodiode detector with a 214 nm bandpass filter. These cross-sections were used in monitoring the MVK and MACR concentrations in the OH kinetic measurements. For these measurements, the MVK and MACR samples were introduced into the absorption cell either by slowly flowing through the absorption cell (MVK/He mixture, 6 s residence time) or using static fills (MACR). All cross-section measurements obeyed Beer's law.

2.3. Photolysis quantum yield measurements

The photolysis quantum yields of MVK and MACR were measured at 298 K using pulsed laser photolysis at 308 (XeCl excimer laser), 337 (N_2 laser), and 351 (XeF excimer laser) nm. The lasers were operated at 10 Hz. Photolysis was performed in a small volume Pyrex cell (i.d., 0.8 cm; length, 27 cm) with quartz windows. The photolysis beam passed along the length of the cell and irradiated the total volume of the cell uniformly. The laser fluence was monitored at the exit of the cell with a thermopile. The laser fluence was varied over the range 6–140 mJ cm^{-2} $pulse^{-1}$.

The loss of MVK or MACR was measured following the photolysis using gas chromatographic (GC) analysis with a non-polar capillary column (DB-5). Due to the small absorption cross-sections of MVK and MACR, $\sim (4\text{–}7) \times 10^{-20}$ cm^2 $molecule^{-1}$, and small quantum yields (see below) at the photolysis wavelengths, the loss of MVK or MACR per pulse was small, $< 10^{-4}$. The fraction of MVK or MACR photolyzed per pulse is given by $\sigma(\lambda) \cdot \Phi(\lambda) \cdot F$, where $\sigma(\lambda)$ is the absorption cross-section of the compound (cm^2 $molecule^{-1}$), $\Phi(\lambda)$ is the quantum yield, and F is the laser fluence per pulse (photons cm^{-2}). The fraction of the MVK sample remaining after one photolysis pulse is:

$$[MVK]_1/[MVK]_0 = 1 - \sigma(\lambda) \cdot \Phi(\lambda) \cdot F \quad (5)$$

where $[MVK]_1$ is the concentration following photolysis and $[MVK]_0$ is the initial concentration. For n photolysis pulses we have:

$$[MVK]_n/[MVK]_0 = (1 - \sigma(\lambda) \cdot \Phi(\lambda) \cdot F)^n \quad (6)$$

For small fractional photolysis this is approximated by:

$$\ln([MVK]_n/[MVK]_0) = -n \cdot \sigma(\lambda) \cdot \Phi(\lambda) \cdot F \quad (7)$$

Therefore, a plot of $\ln([MVK]_n/[MVK]_0)$ vs. n yields a slope equal to $\sigma(\lambda) \cdot \Phi(\lambda) \cdot F$ from which the quantum yields can be obtained using the known MVK absorption cross-section and the measured laser fluence.

The quantum yield measurements were made in the following manner. The cell was filled with the sample in the concentration range 10^{15}–10^{16} molecule cm^{-3}. The total pressure in the cell was brought up to either 25 or 650 Torr with synthetic air (25% O_2 and 75% N_2). The sample was then photolyzed for a measured number of laser shots while monitoring the laser energy transmitted through the cell. After photolysis, a small fraction of the mixture was taken out and the concentration of the photolyte was measured. The sequence of photolysis and concentration measurements was repeated six to eight times for each sample.

The laser fluence was calibrated at each of the photolysis wavelengths using NO_2 as a reference. The NO_2 photolysis quantum yield in this wavelength region is one. However, the O atom produced in the photolysis reacts with NO_2 making the effective quantum yield for loss of NO_2 equal to 2. NO_2 was added to the cell ($\sim 3 \times 10^{16}$ molecule cm^{-3}) and diluted with 50 Torr He. The NO_2 loss was monitored by UV absorption at 366 nm ($\sigma(\lambda) = 5.7 \times 10^{-19}$ cm^2 $molecule^{-1}$ [16]) using a Hg pen ray lamp and monochromator/PMT. The NO_2 cross-sections at the photolysis wavelengths were taken from DeMore et al. [16]. The calibrations were carried out at laser fluences of less than 4 mJ cm^{-2} $pulse^{-1}$. It was assumed that the laser energy meter was linear up to the energies used for the MVK and MACR photolysis measurements.

2.3.1. Materials

UHP He (>99.9999%) and UHP N_2 (99.999%) buffer gases were used in the kinetic measurements. H_2O_2 was purified to ~90% by bubbling He through the sample for several days. The MVK and MACR samples had a manufacturers stated purity of >99%. The samples were vacuum distilled to remove the hydroquinone stabilizer prior to making up gas mixtures. The pressures in the absorption cells and reaction cell were measured using either 10, 100, or 1000 Torr capacitance manometers.

3. Results and discussion

The results obtained for the rate coefficient measurements of reactions (1) and (2), the UV absorption cross-sections, and the photolysis quantum yields are presented separately below.

3.1. OH rate coefficients

3.1.1. $OH + CH_2C(O)CHCH_2$ (k_1)

The measured values of k_1 and the experimental conditions of the measurements are given in Table 1. k_1 was measured between 232 and 378 K in He and N_2 at total pressures between 16 and 100 Torr. The total gas pressure was found to have no effect on the measured value of k_1. Our 298 K value, 2.03×10^{-11} cm^3 molecule^{-1} s^{-1}, is in good agreement with those measured by Kleindienst et al. [6] using the flash photolysis–resonance fluorescence technique and Atkinson et al. [7] using the relative rate technique (OH + propene; reference reaction) and in reasonable agreement with the data of Cox et al. [8] who used the relative rate technique (OH + ethene; reference reaction) with photolysis of HONO as the OH source. The variation of k_1 with temperature is shown in the Arrhenius form in Fig. 1 along with the weighted linear least-squares fit of this data. The obtained Arrhenius parameters are given in Table 2. The results from the previous studies are also given in Table 2 for comparison. Kleindeinst et al. [6] measured k_1 at two temperatures above 298 K and their individual values are in good agreement with those measured here. The differences between our Arrhenius parameters and those reported by Kleindeinst et al. are due to a combination of the scatter in their measurements and the limited number of temperatures used in their study. The differences become the largest when extrapolated to the lowest temperatures of the troposphere, ~200 K. Our value, k_1(200 K), is a factor of 1.5 larger than that obtained using the Kleindeinst et al. [6] parameters.

3.1.2. $OH + HC(O)CH(CH_3)CH_2$ (k_2)

The values of k_2 obtained by us and the conditions of the measurements are given in Table 3. H_2O_2 photolysis at 266 nm was the only OH source used in these measurements. The rate coefficients were found to be independent of the total pressure varied between 20 and 300 Torr. The photolysis laser fluence, and hence the initial $[OH]_o$, was varied by a factor of 4. These variations had no effect on the measured values of k_2. Our 298 K value, 2.79×10^{-11} cm^3 molecule^{-1} s^{-1}, is in good agreement with those measured by Kleindienst et al. [6] and Atkinson et al. [7] but 30% lower than that reported by Edney et al. [9]. The rate coefficients are shown in the

Table 1
Summary of experimental conditions and the measured values of k_1 OH + $CH_2C(O)CH=CH_2$ (MVK) → products

T (K)	$k_1 \pm 2\sigma$ (10^{-11}) (cm^3 molecule^{-1} s^{-1})	[MVK] range (10^{14}) (molecule cm^{-3})	Buffer gas/pressure (Torr)	$[H_2O_2]/[OH]_{t0}$ ($10^{13}/10^{10}$) (molecule cm^{-3})
378	1.35 ± 0.12	0.87–8.92	N_2/100	13.6/6
	1.36 ± 0.12	1.28–12.5	N_2/100	13.4/2
	1.28 ± 0.08	1.02–9.69	N_2/100	14.1/10
354	1.66 ± 0.12	1.19–10.3	He/35	20.1/5
	1.51 ± 0.03	2.35–9.51	He/16	34.6/8
	1.64 ± 0.10	1.38–10.0	He/100	29.4/7
351	1.52 ± 0.14	1.66–12.9	He/26	27.4/13
	1.46 ± 0.07	1.34–12.4	N_2/100	8.8/5
	1.55 ± 0.12	2.15–12.5	N_2/100	25.2/15
323	1.86 ± 0.13	1.85–12.6	N_2/100	17.6/7
	1.73 ± 0.10	1.06–12.9	N_2/100	6.0/4
298	2.01 ± 0.07	0.80–19.7	N_2/100	7.5/5
	1.99 ± 0.12	1.0–20.6	N_2/50	8.7/6
	2.18 ± 0.30	1.84–8.79	N_2/100	21.2/9
	2.02 ± 0.12	1.62–9.81	N_2/100	28.2/13
	1.96 ± 0.08	1.84–21.2	N_2/100	8/7
Average	2.03 ± 0.17 [a]			
272	2.76 ± 0.16	1.21–9.81	N_2/100	26/14
	2.57 ± 0.09	2.25–21.9	N_2/100	13.5/11
253	3.08 ± 0.13	1.51–11.9	N_2/100	12.1/8
	3.16 ± 0.18	1.82–12.0	N_2/100	17/8
	2.80 ± 0.16 [b]	1.75–11.6	N_2/100	3.8/4
	2.83 ± 0.19 [b]	1.62–7.84	N_2/100	5.1/2–8
235	3.65 ± 0.34 [b]	1.07–7.85	N_2/100	6.9/2
232	3.86 ± 0.22	1.18–8.36	N_2/100	6.2/4

[a] Average 298 K value. Values measured over the range 295–299 K have been corrected using $E/R = -612$ K.
[b] OH source: 248 nm photolysis of H_2O_2. All other measurements used 266 nm photolysis.
Quoted uncertainties are the precision of the measurement.

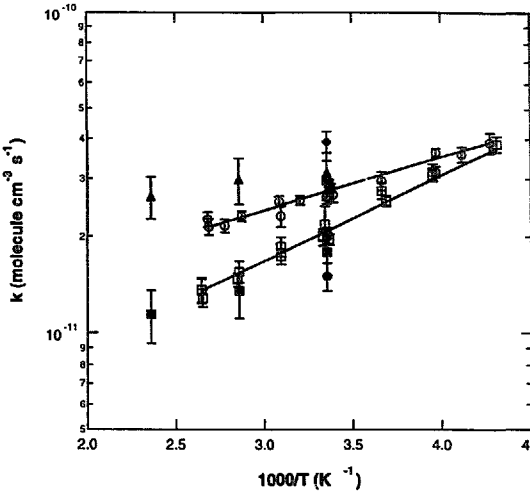

Fig. 1. Arrhenius plots for OH + MVK, k_1, (□) and OH + MACR, k_2, (○). The error bars are the 2σ limits of the measurement precision. The solid lines are the weighted least-squares fits to the data. Also shown are the values reported by Kliendienst et al. [6], MVK (■) and MACR (▲); Atkinson et al. [7] MVK (▽) and MACR (bowtie); Cox et al. [8], MVK (●); Edney et al. [9], MACR (◆).

Table 2
Measurements of k_1 OH + $CH_3C(O)CH=CH_2$ (MVK) → products

k_1(298 K) × 10^{11} (cm^3 molecule^{-1} s^{-1})	$A \times 10^{12}$ (cm^3 molecule^{-1} s^{-1})	$E/R \pm \Delta(E/R)$ (K)	T (K)	Technique [a]	Ref.
1.69 [b]	–	–	300	RR (ethene: 8.0×10^{-12}; 9×10^{-12})	[8]
1.79 ± 0.28	3.85	-456 ± 73	298–424	FP–RF	[6]
2.33 ± 0.18 [b]	–	–	299 ± 2	RR (propene: 2.52×10^{-11}; 3.0×10^{-11})	[7]
2.03 ± 0.17	2.67 ± 0.45	-612 ± 49	232–378	PP–PLIF	This work

[a] RR, relative rate (reference molecule, rate coefficient used, currently recommended rate coefficient (cm^3 molecule^{-1} s^{-1})); FP–RF, flash photolysis resonance fluorescence; PP–PLIF, pulsed photolysis–pulsed laser induced fluorescence.
[b] Room temperature values normalized to the currently recommended [24] reference molecule rate coefficient.

Arrhenius form in Fig. 1. As in the case of k_1, Kleindienst et al. [6] are the only ones who have measured k_2 as a function of temperature. They measured k_2 at two temperatures above 298 K. Their Arrhenius parameters are smaller than those measured here. As pointed out earlier, we did not see any loss of MACR at any temperatures of this study. Therefore, our lower values at $T > 298$ K could not be due to a loss of MACR. Further, our data fits nicely to the Arrhenius expression. The reason for the discrepancy between the two studies is not clear. Table 4 compares our values with the Arrhenius parameters and room temperature values reported in previous studies.

Both MVK and MACR are unsaturated organic compounds, and the reaction with OH is expected to proceed by addition to the C=C double bond. In the case of MACR, the abstraction of the aldehydic H atom is also a likely pathway. Product studies of reactions (1) and (2) at room temperature by Atkinson et al. [7] have shown the importance of these different reaction channels. The conclusions from their studies are that for MVK, OH adds almost exclusively to the terminal C atom. For MACR, OH adds 50% of the time and abstracts the aldehydic H atom 50% of the time at 298 K. Of the OH radicals which add, 80% add to the terminal C atom and 20% add to the secondary C atom. Our measured rate coefficients for both MVK and MACR were found to be independent of pressure, over the range 20–300 Torr, at all the temperatures studied. Also the rate coefficients are well represented by a simple Arrhenius expression over the range

Table 3
Summary of experimental conditions and the measured values of k_2 OH + $CH_2C(CH_3)CHO$ (MACR) → products

T (K)	$k \pm 2\sigma$ (10^{-11}) (cm^3 molecule^{-1} s^{-1})	[MACR] range (10^{14}) (molecule cm^{-3})	Buffer gas/pressure (Torr)	$[H_2O_2]/[OH]_0$ ($10^{11}/10^{10}$) (molecule cm^{-3})
373	2.26 ± 0.12	0.98–9.34	He/20	17/14
372	2.14 ± 0.12	0.56–7.93	He/100	6.5/4
360	2.16 ± 0.10	0.62–9.18	He/100	8/5
348	2.31 ± 0.08	0.58–7.87	He/100	6.9/6
324	2.56 ± 0.10	0.75–8.50	He/100	16.3/11
	2.31 ± 0.14	0.48–9.99	He/100	8.5/9
312	2.58 ± 0.08	0.80–7.79	He/100	16.3/11
298	2.65 ± 0.06	1.05–9.74	N_2/100	10.6/10
	2.93 ± 0.07	0.76–7.76	He/20	24.0/20
	2.85 ± 0.08	0.97–8.81	He/100	47/44
	2.82 ± 0.08	0.71–8.59	He/100	7.5/8
	2.69 ± 0.14	0.82–9.06	He/300	6.2/73
Average	2.79 ± 0.12 [a]			
273	2.97 ± 0.20	0.70–7.98	He/100	6.3/4
252	3.63 ± 0.12	0.78–7.95	He/100	21.2/14
	3.16 ± 0.12	0.68–8.39	He/100	4.8/2
243	3.58 ± 0.20	0.88–8.73	He/100	18/10
234	3.90 ± 0.29	0.99–9.15	He/100	14.2/8

[a] Average 298 K value. Values measured over the range 295–299 K have been corrected using $E/R = -379$ K.
Quoted uncertainties are the precision of the measurement.

Table 4
Measurements of k_2 OH + $CH_2C(CH_3)CHO$ (MACR) → products

k_2(298 K) × 10^{11} (cm^3 molecule^{-1} s^{-1})	$A \times 10^{12}$ (cm^3 molecule^{-1} s^{-1})	$E/R \pm \Delta(E/R)$ (K)	T (K)	Technique [a]	Ref.
3.14 ± 0.49	17.7	−175 ± 52	300–423	FP–RF	[6]
3.52 ± 0.28 [b]	–	–	299 ± 2	RR (propene: 2.52×10^{-11}; 3.0×10^{-11})	[7]
4.43 ± 0.35 [b]	–	–	298	RR (propene: 2.65×10^{-11}; 3.0×10^{-11})	[9]
2.79 ± 0.12	7.73 ± 0.65	−379 ± 46	234–373	PP–PLIF	This work

[a] RR, relative rate (reference molecule, rate coefficient used, currently recommended rate coefficient (cm^3 molecule^{-1} s^{-1})); FP–RF, flash photolysis resonance fluorescence; PP–PLIF, pulsed photolysis–pulsed laser induced fluorescence.
[b] Room temperature values normalized to the currently recommended [24] reference molecule rate coefficient.

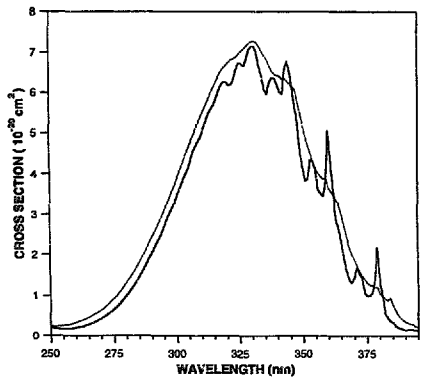

Fig. 2. Absorption spectra of MVK (——) and MACR (——) at 298 K.

of temperatures used in the present study. Therefore, the addition channels for these bimolecular rate coefficients must be at their high pressure limiting value.

3.1.3. UV absorption spectra

The room temperature absorption spectra for both MVK and MACR are shown in Fig. 2 over the wavelength range 250–395 nm. Tables of the cross-sections at 1 nm intervals are available from the authors. The absorption spectra of MVK and MACR are very similar in terms of the peak positions, absorption cross-sections, and band widths (FWHM). This is expected because the molecular structures of these two molecules are similar. The most prominent difference between the two spectra is the magnitude of the vibrational band structure which is superimposed on the continuum envelope. The vibrational band structure is much stronger in the MACR spectrum than that of MVK. The vibrational progression begins in the long wavelength tail of the spectrum and extends to near 310 nm. The disappearance of the vibrational

structure in the short wavelength region indicates a possible threshold for the photodissociation or predissociation of the excited state. The continuous nature of the spectrum at short wavelength implies a purely dissociative transition. A detailed analysis of the vibrational band structure has been reported by Birge et al. [11,12].

Our cross-section measurements are in reasonable agreement, ~10%, with those of Raber and Moortgat [10] (taken from their Fig. 1). Raber and Moortgat report the peak absorption of MACR to be slightly higher than that of MVK by ~10%. Our measurements found the peak cross-sections for these molecules to be almost identical with an average value of $\sim 7.2\times10^{-20}$ cm^2 molecule^{-1}. Our peak cross-section values lie between the values reported by Raber and Moortgat for MVK, $\sim 6.5\times10^{-20}$ cm^2, and MACR, $\sim 7.5\times10^{-20}$ cm^2. These differences lie just outside of our estimated uncertainties.

Measurements of the absorption cross-sections were also made at reduced temperatures over the range 250–298 K. The peak cross-sections showed a small increase with decreasing temperature. The peak cross-section of MVK increased by <2% at 250 K. The vibrational band features also became slightly sharper at reduced temperature. Otherwise the shape of the absorption band was relatively insensitive to temperature. Therefore, the temperature dependence of the absorption spectrum is not expected to be important in the atmosphere.

Both MVK and MACR show strong absorption bands at shorter wavelengths. The onset of these absorption bands is slightly different for the two molecules. MACR shows stronger absorption at 214 nm by more than a factor of 3. The absorption cross-sections at 214 nm are $(6.6\pm0.04)\times10^{-18}$ cm^2 and $(2.21\pm0.03)\times10^{-17}$ cm^2 for MVK and MACR respectively. Fahr et al. [17] have recently reported absorption cross-sections for MVK over the wavelength range 160–260 nm. Their cross-section at 214 nm is in good agreement, ±10%, with our value. The short wavelength absorption bands do not play an important role in the atmospheric photolysis of MVK or MACR.

3.1.4. Photolysis quantum yields

The photolysis quantum yield was determined by monitoring the loss rate of the parent compound. A potential weakness in this approach is the occurrence of unwanted secondary reactions which could remove the parent compound. To minimize secondary reactions, O_2 was added in large excess over MVK and MACR. O_2 converted reactive radical species to peroxy radicals ($k_z \sim 10^{-12}$ cm^3 molecule^{-1} s^{-1}, Atkinson [18]), which are not expected to react with MVK or MACR [19]. Therefore, the disappearance of the parent compound in the presence of O_2 should be a good measure of the photodissociation process. The invariance of the measured quantum yields with laser repetition rate and a very small dependence on laser fluence (see below) also support this contention. Yet, conservatively, we report quantum yields as upper limits.

Quantum yield measurements were made using 308, 337, and 351 nm photolysis at total pressures of 25 and 650 Torr and over a range of laser fluences. The results of these measurements are summarized in Table 5. The measured quantum yields increased a little with laser fluence, i.e. there was a small contribution due to secondary chemistry. The measured quantum yields were extrapolated to zero laser energy to estimate the true quantum yield, $\Phi_0(\lambda)$. For MACR, $\Phi_0(\lambda)$ was very small and, therefore, could not be accurately determined. No dependence on total pressure or photolysis wavelength was observed. Therefore, we recommend a value of $\Phi(\text{MACR}) < 0.01$ for dissociation of MACR at all wavelengths greater than 308 nm.

The quantum yields for MVK removal depend on both wavelength and pressure. At 351 nm, the $\Phi_0(\lambda)$ values at 25 and 650 Torr were <0.01 with no measurable pressure dependence. However, at 308 nm the $\Phi_0(\lambda)$ values decreased with increasing pressure; it was 0.16 at 25 Torr and 0.04 at 650 Torr. At 337 nm, $\Phi_0(\lambda)$ varied slightly with pressure and it was between the values observed at 308 and 351 nm.

For atmospheric model calculations, we have fit our limited data to an expression where the quantum yield varies inversely with pressure, Stern–Volmer type analysis, and exponentially with wavelength beyond a threshold for dissociation:

$$\Phi_0(\lambda,P) < \exp[-0.055(\lambda-308)]/(5.5+9.2\times10^{-19}N) \quad (8)$$

In the above expression λ is in nm and N is the number density in molecule cm^{-3}. This expression reproduces the experimental data within the quoted uncertainties.

Raber and Moortgat [10] have reported MVK and MACR photolysis quantum yields. They quote $\Phi<0.03$ for MACR and $\Phi<0.05$ for MVK at 1 atm. They monitored the appearance of products by longpath Fourier transform infrared spectrometry (FTIR) following broadband photolysis, which did not allow them to obtain wavelength dependent quantum yields. Their quoted upper limits are consistent with our results.

End products of MVK and MACR photolysis were measured using GC and GC/MS analysis. CO_2 and CO, the expected major end products, were not measured. Our analysis was limited to quantification of hydrocarbons and identification of oxygenated compounds. The major end products observed in MACR photolysis were: methane, ethylene, acetylene, allene and propyne. Minor products such as formaldehyde, methanol, formic acid, acetic acid and hydroxyacetone were also observed. Propylene and dimethylketene (DMK) were not observed. Major photolysis end products in MVK photolysis were acetylene, propylene and methanol, with minor products being methane, ethane, ethylene, formaldehyde, acetone or propanal, formic acid, and acetic acid.

In general, the products we observed are consistent with those in previous studies. Similar to the results of Raber and Moortgat [10], we find the major products of MVK photol-

Table 5
MACR and MVK photolysis quantum yield data

Photolysis wavelength (nm)	Total pressure (Torr)	Laser fluence (mJ cm^{-2} pulse^{-1})	$\Phi \pm 2\sigma$	$\Phi_0 \pm 2\sigma$
MACR				
308	650	122	0.032 ± 0.008	
		90	0.029 ± 0.002	
		56	0.019 ± 0.004	0.008 ± 0.001
		26	0.013 ± 0.004	
		8	0.010 ± 0.006	
	25	128	0.11 ± 0.02	
		90	0.10 ± 0.03	
		54	0.04 ± 0.02	0.005 ± 0.01
		6	0.01 ± 0.01	
351	650	118	0.013 ± 0.003	
		70	0.01 ± 0.002	
		28	0.006 ± 0.002	0.005 ± 0.002
		10	0.006 ± 0.001	
	25	92	0.03 ± 0.004	
		54	0.02 ± 0.003	
		28	0.006 ± 0.003	0.003 ± 0.004
		8	0.008 ± 0.003	
MVK				
308	650	142	0.033 ± 0.002	
		106	0.042 ± 0.006	
		72	0.026 ± 0.006	0.04 ± 0.015
		26	0.049 ± 0.008	
		8	0.036 ± 0.004	
	25	130	0.20 ± 0.02	
		100	0.18 ± 0.02	
		68	0.18 ± 0.02	0.16 ± 0.015
		52	0.18 ± 0.02	
		34	0.18 ± 0.02	
		6	0.15 ± 0.02	
337	650	3	0.008 ± 0.003	
	25	3	0.04 ± 0.01	
351	650	130	0.009 ± 0.002	
		80	0.007 ± 0.001	
		46	0.004 ± 0.0005	0.003 ± 0.002
		8	0.004 ± 0.00	
	25	134	0.050 ± 0.006	
		90	0.037 ± 0.006	
		48	0.016 ± 0.003	0.01 ± 0.01
		6	0.015 ± 0.002	

Uncertainties are measurement precision only.

ysis to be propylene, acetylene and methanol. They concluded the major primary photolysis products of MVK to be $CH_3CHCH_2 + CO$.

For MACR, propylene has been identified as a major product in previous studies but it was not observed here. Johnstone and Sodeau [20] photolyzed MACR in an Ar matrix at wavelengths greater than 300 nm, and observed only small changes in composition. They concluded MACR underwent only trans–cis isomerization. Below 230 nm propene, DMK, and DMM (dimethylmethylene) and CO were observed.

Fahr et al. [17] have recently studied the photolysis of MVK at 193 nm. They observed a unit quantum yield for its loss with the primary photolysis product being CH_3CO. Photolysis at 193 nm, however, probes a different electronic transition than studied here.

4. Atmospheric implications

Kinetic parameters for reactions with OH, O_3, NO_3 and the quantum yield for dissociation have been used to calculate the atmospheric lifetimes of MVK and MACR. Fig. 3 shows the atmospheric loss rates as a function of altitude at 30°N for MACR and MVK. The solar flux is diurnally averaged for the summer with 300 Dobson units of O_3 with the OH concentration calculated for these conditions [21]. The MACR photolysis quantum yields were taken as 0.01 (our upper limit) while the MVK quantum yields were calculated using Eq. (8). Reactive loss of MACR and MVK with OH is the dominant loss process for both MACR and MVK from the boundary layer through the upper troposphere. Reaction of MACR and MVK with O_3 or NO_3 does not contribute

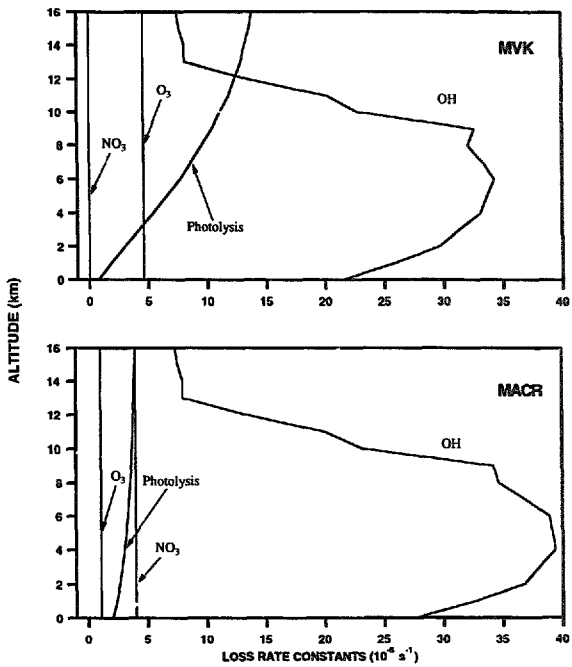

Fig. 3. Atmospheric loss rates constants of MACR and MVK as a function of altitude. The reactive losses were calculated using: $[O_3] = 1 \times 10^{12}$ molecule cm^{-3} with $k_{MACR} = 1.1 \times 10^{-18}$ cm^3 molecule^{-1} s^{-1}, $k_{MVK} = 4.6 \times 10^{-18}$ cm^3 molecule^{-1} s^{-1} [10]; $[NO_3] = 5 \times 10^8$ molecule cm^{-3} with $k_{MACR} = 8 \times 10^{-15}$ cm^3 molecule^{-1} s^{-1}, $k_{MVK} = 1.2 \times 10^{-16}$ cm^3 molecule^{-1} s^{-1} [22]; and [OH] calculated for summer at 30 N with the rate constants quoted in this work.

significantly [10,22]. Therefore, photolysis is not a significant loss process for MACR and only a minor process for MVK.

The tropospheric lifetimes of MACR and MVK fall in the range 6–10 h. Therefore, these species are rapidly processed in the troposphere on a local scale and do not impact on regional scale chemistry directly. However, the oxidized products formed from these species (i.e. PAN [23]) will have a regional impact.

Acknowledgements

We thank Dr. S.A. Montzka for providing a calibrated mixture of methyl vinyl ketone in He and preforming GC/MS sample analysis. This research was funded in part by NOAA's Climate and Global Change Research Program.

References

[1] W.L. Chameides, R.W. Lindsay, J. Richardson, C.S. Kiang, Science 241 (1988) 1473.
[2] M. Trainer, E.J. Williams, D.D. Parrish, M.P. Buhr, E.J. Allwine, H.H. Westberg, F.C. Fehsenfeld, S.C. Liu, Nature 329 (1987) 705.
[3] D. Pierotti, S.C. Wofsy, D. Jacob, R.A. Rasmussen, J. Geophys. Res. 95 (1990) 1871.
[4] R.S. Martin, H. Westberg, E. Allwine, L. Ashman, J. Carl Farmer, B. Lamb, J. Atmos. Chem. 13 (1991) 1.
[5] S.A. Montzka, M. Trainer, P.D. Goldan, W.C. Kuster, F.C. Fehsenfeld, J. Geophys. Res. 1 (1992) 1101.
[6] T.E. Kleindienst, G.W. Harris, J.N. Pitts, Jr., Environ. Sci. Technol. 16 (1982) 844.
[7] R. Atkinson, S.M. Aschman, J.N. Pitts, Jr., Int. J. Chem. Kinet. 15 (1983) 75.
[8] R.A. Cox, R.G. Derwent, M.R. Williams, Environ. Sci. Technol. 14 (1980) 57.
[9] E.O. Edney, T.E. Kleindienst, E.W. Corse, Int. J. Chem. Kinet. 18 (1986) 1355.

[10] W.H. Raber, G.K. Moortgat, in: J. Barker (ed.), Adv. Series Phys. Chem., Progress and problems in atmospheric chemistry, World Scientific, Singapore, 1995, p. 318.
[11] R.R. Birge, W.C. Pringle, P.A. Leermakers, J. Am. Chem. Soc. 93 (1971) 6715.
[12] R.R. Birge, P.A. Leermakers, J. Am. Chem. Soc. 94 (1972) 8105.
[13] G.L. Vaghjiani, A.R. Ravishankara, J. Chem. Phys. 93 (1989) 1948.
[14] J.B. Burkholder, R.K. Talukdar, A.R. Ravishankara, S. Solomon, J. Geophys. Res. 98 (1993) 22 937.
[15] G.L. Vaghjiani, A.R. Ravishankara, J. Chem. Phys. 92 (1990) 996.
[16] W.B. DeMore, S.P. Sanders, D.M. Golden, R.F. Hampson, M.J. Kurylo, C.J. Howard, A.R. Ravishankara, C.E. Kolb, M.J. Molina, Chemical kinetics and photochemical data for use in stratospheric modeling, Evaluation 11, JPL Publ., Vol. 94-26, 1994.
[17] A. Fahr, W. Braun, A.H. Laufer, J. Phys. Chem. 97 (1993) 1502.
[18] R. Atkinson, J. Phys. Chem. Ref. Data, Monograph 2 (1994) 175.
[19] A.C. Lloyd, Int. J. Chem. Kinet. 6 (1974) 163.
[20] D.E. Johnstone, J.R. Sodeau, J. Chem. Soc. Faraday Trans. 88 (1992) 409.
[21] S. McKeen, private communication.
[22] Y. Rudich, R.K. Talukdar, R.W. Fox, A.R. Ravishankara, J. Phys. Chem. 100 (1996) 5374.
[23] R.K. Talukdar, J.B. Burkholder, A.-M. Schmoltner, J.M. Roberts, R.R. Wilson, A.R. Ravishankara, J. Geophys. Res. 100 (1995) 14163.
[24] R. Atkinson, D.L. Baulch, R.A. Cox, R.F. Hampson, Jr., J.A. Kerr, M.J. Rossi, J. Troe, J. Phys. Chem. Ref. Data, 26 (1997) 521.